Supercoupling between heavy-hole and light-hole states in nanostructures

Jun-Wei Luo,[1,2,*] Gabriel Bester,[3] and Alex Zunger[4]

[1]*State Key Laboratory of Superlattices and Microstructures, Institute of Semiconductors, Chinese Academy of Sciences, Beijing 100083, China*

[2]*Synergetic Innovation Center of Quantum Information and Quantum Physics, University of Science and Technology of China, Hefei, Anhui 230026, China*

[3]*Max-Planck-Institut für Festkörperforschung, Heisenbergstrasse 1, D-70569 Stuttgart, Germany*

[4]*Renewable and Sustainable Energy Institute, University of Colorado, Boulder, Colorado 80309, USA*

(Received 22 July 2015; published 1 October 2015)

The heavy-hole (HH) and light-hole (LH) components of the valence states in three-dimensional (3D) bulk semiconductors can mix quantum mechanically as the dimensionality is reduced in forming low-D nanostructures, such as 2D quantum wells, 1D quantum wires, and 0D quantum dots (QDs). This coupling controls the tuning of the excitonic fine-structure splitting, provides an efficient channel for the spin coherence, and leads to polarization anisotropy of light emission, central to several quantum-information schemes. The current understanding is that the mixing scales with the square of $\delta V_{\rm HL}/\Delta_{\rm HL}$, where $\delta V_{\rm HL}$ and $\Delta_{\rm HL}$ are the coupling matrix elements of the crystal potential and the energy separation between the primary HH0 and LH0 states, respectively. We discuss two classes of HH-LH coupling mechanisms. First, coupling factors occurring through the numerator $\delta V_{\rm HL}$, referred to as "direct coupling," including the well-known (i) quantum confinement, (ii) built-in strain, and (iii) shape elongation, as well as three additional direct coupling mechanisms discussed here: (iv) the intrinsic C_{2v} crystal-field effect, (v) the local symmetry of the interface, and (vi) the alloy disorder. We quantify these six direct HH-LH coupling effects by performing atomistic pseudopotential calculations on a range of strained and unstrained QDs of different morphologies. We find that in unstrained self-assembled QDs such as GaAs/AlGaAs, effects (i)–(vi) contribute 0%, 0%, 0%, 0%, 40%, and 60%, respectively, whereas in strained self-assembled QDs such as InGaAs/GaAs they contribute 0%, 0%, 78%, 0%, 8%, and 14%, respectively, to the direct HH-LH coupling $\delta V_{\rm HL}$. These relative contributions to direct HH-LH coupling differ significantly from what was previously believed. Second, we discover an unexpected HH-LH supercoupling that effectively reduces the denominator $\Delta_{\rm HL}$ by the presence of a dense ladder of intermediate states between the HH0 and LH0 states (analogous to superexchange in magnetism). Supercoupling amplifies and propagates the HH-LH interaction and is the dominant source of HH-LH mixing in strained nanostructures where $\Delta_{\rm HL}$ is fairly large, so by the direct coupling mechanism alone $\delta V_{\rm HL}/\Delta_{\rm HL}$ would be expected to be rather small. Supercoupling explains a number of outstanding puzzles, including the surprising fact that in strained (InAs/GaAs) QDs the mixing is very strong despite the fact that $\Delta_{\rm HL}$ is large, and it offers a way to manipulate HH-LH mixing and hence associated properties in nanostructures.

DOI: 10.1103/PhysRevB.92.165301 PACS number(s): 73.22.−f, 74.20.Pq, 78.67.Hc

I. INTRODUCTION

The reduced symmetry in low-dimensional nanostructures with respect to three-dimensional (3D) bulk crystals offers the possibility of quantum mixing between the "heavy-hole" (HH) and "light-hole" (LH) components of the bulk Γ_{8v} valence band. The two components of the valence band have diametrically opposed fundamental features (including different Bloch functions, pseudospin, type of optical transition, magnitude of effective masses, and deformation potentials), so the extent of their quantum-mechanical mixing underlies our fundamental understanding of the duality of a broad range of physical properties associated with holes in low-dimensional nanostructures. Specifically, such HH-LH mixing plays important roles in, e.g., quantum dots (QDs) [1], including (i) tuning of the excitonic fine-structure splitting [2–4], which controls the fidelity of entangled photon pairs; (ii) providing an efficient channel for spin decoherence [5–10]; (iii) creating a polarization anisotropy of light emission, which is important for quantum-information schemes [11–15]; and (iv) giving an additional efficient mechanism for optical initialization of a hole spin qubit [16,17]. The origin of this mixing has fascinated physicists and chemists ever since low-dimensional semiconductor nanostructures such as 2D quantum wells, 1D quantum wires, and 0D QDs were made [11–13,18], yet the controlling mechanisms are rather vague. Numerical calculations of QDs including $\mathbf{k}\cdot\mathbf{p}$ [19] did include a numbers of HH-LH coupling mechanisms, but they have not elucidated individual characteristics of coupling mechanisms.

The HH-LH mixing is qualitatively expected to scale as $(\delta V_{\rm HL}/\Delta_{\rm HL})^2$ in terms of the classic "folded down" approach [5], where $\delta V_{\rm HL} = \langle {\rm LH0}|\delta V|{\rm HH0}\rangle$ is the matrix element of the crystal potential and $\Delta_{\rm HL}$ is the energy separation between the primary HH0 and LH0 states. The most popular theoretical approach used in nanostructures is to fold the Luttinger-Kohn $\mathbf{k}\cdot\mathbf{p}$ or Pikus-Bir strained Hamiltonian of bulk zinc-blende (ZB) semiconductors down to an effective 2×2 HH Hamiltonian, taking the admixture of neighboring bands such as the LH band into account perturbatively [5–9,20]. In the early days of nanostructures research, HH-LH mixing was depicted as a result of spatial quantum confinement [5,14,21–25], which leads to finite off-diagonal matrix elements within the Luttinger-Kohn $\mathbf{k}\cdot\mathbf{p}$

*jwluo@semi.ac.cn

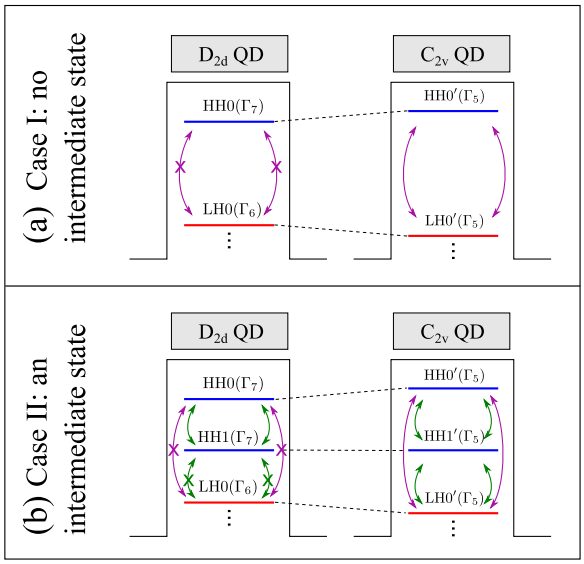

FIG. 1. (Color online) (a) In case I, the QD has no intermediate states lying between the HH0 and LH0 states. (b) Case II is usually in strained QDs where strain-induced large HH-LH splitting accommodates the existence of intermediate states lying between the HH0 and LH0 states. In D_{2d} symmetry, the coupling between HH and LH states is forbidden, and in C_{2v} such coupling is allowed.

Hamiltonian. However, δV_{HL}, and thus HH-LH mixing, was later recognized to be zero by the symmetry in symmetric self-assembled QDs, which were assumed (incorrectly) to have the D_{2d} point group [11–13,18]. In D_{2d}, the representations of HH and LH are distinct so their coupling vanishes, as shown schematically in Fig. 1(a). Since the quantum confinement argument led to vanishing HH-LH coupling, other effects were invoked. For example, the built-in strain was considered as the origin of observed sizable HH-LH mixing in *strained* QDs such as In(Ga)As/GaAs [12] and CdTe/ZnTe [11] QDs. The nonuniform strain could lower the QD symmetry from D_{2d} to C_{2v}, a group in which all QD states, including HH and LH, belong to the *same* irreducible representation Γ_5, and consequently they are allowed to have a nonzero δV_{HL}, as shown schematically in Fig. 1(a). Surprisingly and inconsistently, considerable HH-LH mixing was recently observed even in *strain-free* epitaxial GaAs/AlGaAs QDs, which are not supposed to distort by strain to C_{2v}. Therefore, an alternative mechanism had to be proposed to solve this puzzle [13]. Researchers postulated that elongation of the dot should exist along one crystal axis, which could lower the dot symmetry to C_{2v}.

However, we demonstrate that the atomic-scale symmetry of the lens or Gaussian shaped self-assembled QDs with cylindrical geometry made of ZB semiconductors is already lowered to C_{2v} even without built-in strain and shape elongation [19,26]. We demonstrate in this work two classes of HH-LH mixing mechanisms. (a) *Direct coupling effects*, including the well-known space confinement, built-in strain, and shape elongation, as well as three additional effects—intrinsic C_{2v} crystal field, local symmetry of interfaces, and alloy disorder—contribute to HH-LH mixing through δV_{HL}. (b) *Supercoupling effect*: an unexpected mechanism (analogous to superexchange in magnetism) magnifying HH-LH mixing through effectively reducing Δ_{HL} by the presence of a dense ladder of intermediate states between the HH0 and LH0 states in nanostructures; see the schematic in Fig. 1(b). In this work, we show how the six direct coupling effects emerge from different mechanisms, and then we discuss the supercoupling effect.

II. THEORETICAL METHODOLOGY

A. The strategy of the methodology

Our strategy for gaining access to the physics determining HH-LH mixing in QDs is to first calculate rather precisely the wave functions in a large range of shapes, compositions, and strains of (Ga,In)As dots in a (Al,Ga)As matrix, using the all-band atomistic pseudopotential method, free from any specific model assumptions on the nature of the HH-LH mixing. We address the QD problem by solving the multimillion atoms QD architecture with atoms located at specific positions, each carrying its own (screened) pseudopotential. The calculated eigenvalues and wave functions are illustrated in Fig. 2. Since we explicitly specify the coordinates of each atom in the nanostructures under consideration, this forces upon us the correct atomically resolved symmetry. We are thus free from the need to prejudge at the outset which 3D bands will couple in nanostructures, a judgment needed in the truncation of the $\mathbf{k}\cdot\mathbf{p}$ expansion. This method has been tested extensively over the past two decades for a broad range of spectroscopic quantities in self-assembled as well as colloidal nanostructures [4,10,27–33]. The well-known $\mathbf{k}\cdot\mathbf{p}$ approaches can also be accurate in principle at the limit of a large number (possibly infinite) of band basis functions [20]. Unfortunately, this would require knowing a large number of (Luttinger-like) coupling parameters that are not provided by $\mathbf{k}\cdot\mathbf{p}$ theory itself but need to be supplied by other, currently unavailable sources. Well-established literature tests [31–33] have shown that even the state-of-the-art $\mathbf{k}\cdot\mathbf{p}$ using eight basis functions and displacing atoms according to atomistic (valence force field) elasticity theory [19] still shows significant deviations from the corresponding all-band pseudopotential description of the same self-assembled InGaAs QDs [33] as well as colloidal CdSe and InP dots [31,32]. Although we believe that a sufficiently complete basis-set $\mathbf{k}\cdot\mathbf{p}$ approach might be able to convey realistically the HH-LH mixing, we wish to circumvent the uncertainties related to the convergence with the number of basis states by using instead the well-tested [4,10,27–33] all-bulk band direct diagonalization approach that treats a QD explicitly as a giant molecule without making the $\mathbf{k}\cdot\mathbf{p}$ expansion. By applying this approach to a broad range of QD shapes, symmetries, and compositions, we found an unexpected mechanism of supercoupling. A simple qualitative perturbative model is then developed to analyze our numerical results (but not to replace them). This model illustrates in a simple manner the physical origin of the supercoupling effect, and it can be used to inspire future model Hamiltonian approaches that capture HH-LH mixing.

B. Computational details

The electronic states of GaAs/Al(Ga)As and In(Ga)As/GaAs QDs are obtained by solving the Schrödinger equation

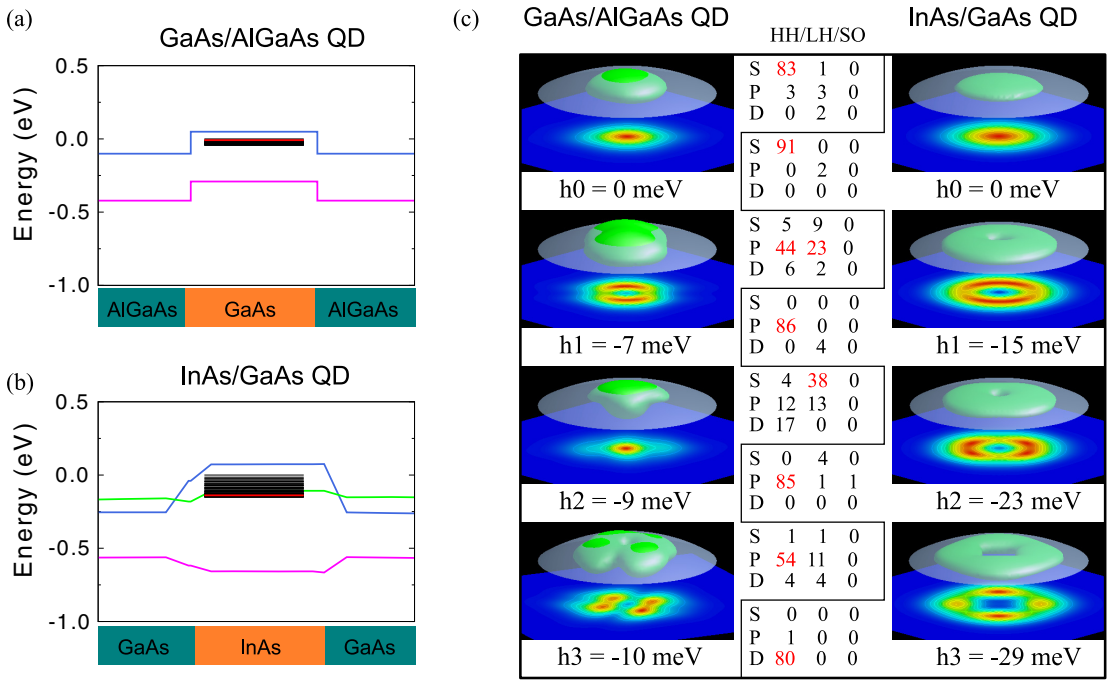

FIG. 2. (Color online) Energy level structure and wave functions of strained and unstrained QDs obtained from direct atomistic calculations. Calculated energy levels of (a) an unstrained GaAs/AlGaAs QD and (b) a strained InAs/GaAs QD. The orange region denotes the QD and green denotes the matrix. Short lines are for QD levels, but the red one highlights the LH-like ground state. Bold lines represent energy alignment of HH (blue), LH (green), and SO (magenta) through the QD center. (c) Square of the wave functions (3D isosurface and 2D in-plane contour plots) of the highest four-hole states for the corresponding GaAs/AlGaAs QD (left column) and InAs/GaAs QD (right column). For analysis purposes, we project the QD wave functions onto the Bloch states of HH, LH, SO, and CB bands at the Γ point of the bulk, and we decompose them with respect to their axial angular momentum components (S,P,D). Both QDs have the same lens shape and size (base diameter 25 nm and 3 nm height). We should note that excited states may contain sizable components out of S,P,D, e.g., the h3 state of the GaAs QD containing a large magnitude of the F component (about 12%), which distorts the wave function away from P-like.

in a crystal (QD+matrix) potential $V(\mathbf{r})$ within a basis of strained bulk Bloch bands [29]. The screened potential $V(\mathbf{r})$ is constructed as a superposition of atomic pseudopotentials $\hat{v}_\alpha$ centered at the atomic positions $\mathbf{R}_{\alpha,n}$ [29], where n is the primary cell site index: $V(\mathbf{r}) = \sum_n \sum_\alpha \hat{v}_\alpha(\mathbf{r} - \mathbf{R}_{\alpha,n})$. This approach captures the multiband and intervalley coupling as well as spin-orbit interactions, and it also forces upon the eigenstates the correct atomistic symmetry of the underlying nanostructure. The atomic pseudopotentials $\hat{v}_\alpha$ are fit to experimental transition energies, effective masses, spin-orbit splittings, and deformation potentials of the underlying bulk semiconductors as well as to band offsets of, e.g., InAs/GaAs heterojunctions [30,34]. The atomistic valence force field (VFF) model [26] is used to find the equilibrium atomic positions $\mathbf{R}_{\alpha,n}$ via minimization of the lattice-mismatch-induced strain energy.

To retrieve the components of bulk bands, we project the precisely computed QD wave functions onto a basis of Bloch states of bulk bands, such as HH $= |3/2,\pm 3/2\rangle$, LH $= |3/2,\pm 1/2\rangle$, SO $= |1/2,\pm 1/2\rangle$, and conduction bands, at the Γ point [35]. Their projection onto bulk Bloch states, as well as their decomposition with respect to their axial angular momentum components (S,P,D), are shown in Fig. 2. From this post-analysis computation of QD wave functions, we find the HH-like and LH-like ground states, HH0 and LH0, respectively. We now obtain (i) the HH-LH splitting Δ_{HL}, which is usually caused by biaxial strain and spatial quantum confinement, and (ii) the LH component in the HH0 state, which is usually the ground hole state of QDs, i.e., the magnitude of the HH-LH mixing λ^2_{LH}. These quantities allow us to unravel the physics of the HH-LH mixing as described below.

III. RESULTS

A. Types of dots considered

We have considered three types of QDs: (i) 36 *strained* In(Ga)As/GaAs QDs [11,12]; (ii) 31 *unstrained* GaAs/Al(Ga)As QDs [13], with varying dot height, shape, base size, and compositions, both belonging to nominal C_{2v} symmetry (here, "nominal symmetry" refers to the QD symmetry excluding alloying effect); and (iii) six *unstrained* nominal D_{2d} GaAs/Al(Ga)As QDs. The types of structures of QDs calculated here are inspired from experimental measurements.

Type (i) dots: In(Ga)As/GaAs QDs are lens-shaped and the dot height varies from 2 to 6 nm. The base of 11 In(Ga)As/GaAs QDs (solid circles in Fig. 3) is symmetric with a 25 nm diameter, and 3 out of 11 are $In_{0.6}Ga_{0.4}As$ alloy QDs. From the remaining 25 InAs/GaAs QDs (open circles in Fig. 3), 12 dots have anisotropic elongation with a base size 25×20, 25×23, 25×28, and 25×30 nm and a dot height of 3, 4, and 5 nm, respectively, and the other 13 QDs are symmetric with a base size from 20 to 26 nm and varying dot height.

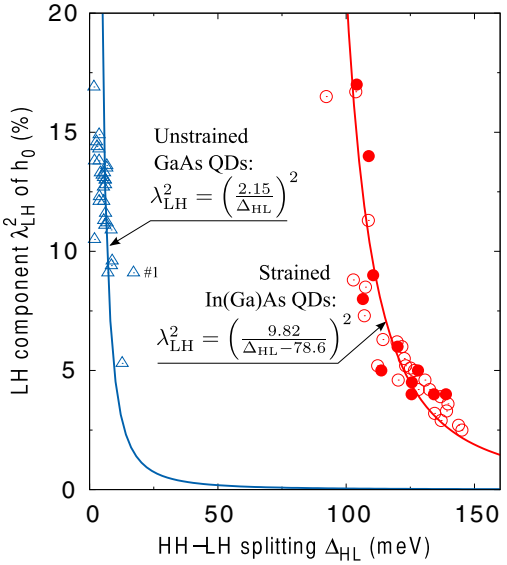

FIG. 3. (Color online) HH-LH mixing strength λ^2_{LH} of the HH-like ground hole state h_0 obtained from direct atomistic calculations for QDs. λ^2_{LH} vs Δ_{HL} for both strained In(Ga)As/GaAs (represented by red dots and circles) and unstrained GaAs/Al(Ga)As QDs (by blue triangles) with varying QD shape, size, and composition. All GaAs/Al(Ga)As QDs have their λ^2_{LH} vs Δ_{HL} values close to a common curve described by Eq. (1) with $\delta V_{HL} = 2.15$ meV, whereas all the data of strained In(Ga)As/GaAs QDs are well described by a common curve given by Eq. (2) with $\delta V_{HL} = 9.82$ meV.

Type (ii) dots: GaAs/Al(Ga)As QDs have five lens-shaped symmetric GaAs/AlGaAs QDs with the same 25 nm base size and varying dot height. The remanding 26 GaAs/AlGaAs QDs are Gaussian-shaped with a base size of 25 nm (11 QDs), 30 nm (5 QDs), and 35×30 nm (5 QDs) and 30x35 nm (5 QDs) for circular and elongated dots, respectively, and varying dot height. *Type (iii) dots:* GaAs QDs are disk-shaped with a 25-nm-diameter base size and dot height varying from 2 to 6 nm. Most of the GaAs QDs are embedded in the $Al_{0.3}Ga_{0.7}As$ matrix, except for three dots in the pure AlAs matrix.

B. Comparison of strained and unstrained QDs–microscopic wavefunctions and energies

We first compare the energy levels and wave functions (see Fig. 2) between *unstrained* GaAs/AlGaAs and *strained* InAs/GaAs QDs with the same dot morphology of lens-shape, 3 nm dot height, and 25 nm base size. In an unstrained GaAs/AlGaAs QD, the LH0 is adjacent to the HH0 with $\Delta_{HL} = 7$ meV, whereas in a strained InAs/GaAs QD, the HH0 is followed by 30 HH-like excited states and then the LH0 gives rise to $\Delta_{HL} = 139$ meV. This contradistinction is a consequence of the strain, which is absent in a GaAs/AlGaAs QD but built-in in an InAs/GaAs QD. As shown in Fig. 2(b), the built-in strain splits the HH and LH bands of InAs/GaAs QDs by as much as $\Delta_{HL} \approx 120$ meV.

C. k · p analysis of atomistic microscopic results

We next carry out the analysis of the precise numerical results via simpler models. The obtained HH-LH mixing λ^2_{LH}

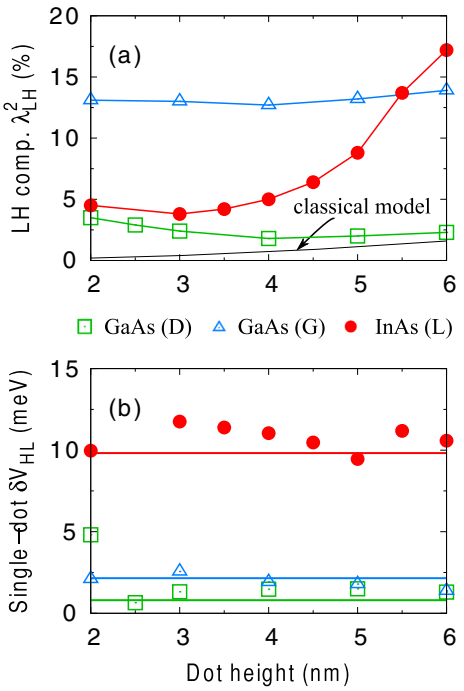

FIG. 4. (Color online) (a) Dependence of λ^2_{LH} of the ground hole state on the QD height for Gaussian-shaped (G) and disk-shaped (D) GaAs/Al(Ga)As QDs and lens-shaped (L) InAs/GaAs QDs with the same 25 nm base size, as well as the results of a classic description for GaAs QDs adopted from Ref. [5]. (b) Dependence of single dot δV_{HL} on the QD height compared with the fitted common δV_{HL} values, which are indicated by bold lines, for the corresponding QD classes.

as a function of the HH-LH splitting Δ_{HL} is shown in Fig. 3 for 31 unstrained C_{2v} GaAs/Al(Ga)As QDs and 36 strained In(Ga)As/GaAs QDs. As shown in Fig. 3, in the class of unstrained C_{2v} GaAs/AlGaAs QDs, the λ_{LH} values of all such QDs fall close to a common curve of

$$\lambda_{LH} = \frac{\delta V_{HL}}{\Delta_{HL}}, \tag{1}$$

with a *common* coupling matrix element $\delta V_{HL} = 2.15$ meV, despite their different shapes, sizes, and compositions. This formula is expected from the classical "folded down" perturbation approach [1–7,11–14,16]. On the other hand, all data points of strained In(Ga)As/GaAs QDs exhibit a denominator Δ_{HL} that is effectively reduced by $\delta = 78.6$ meV with respect to the class of unstrained GaAs QDs, and they fall then close to another curve:

$$\lambda_{LH} = \frac{\delta V_{HL}}{(\Delta_{HL} - \delta)}, \tag{2}$$

whereas its numerator is enhanced to $\delta V_{HL} = 9.82$ meV. This result is unexpected in the commonly used "folded down" concept. It is interesting to note that all GaAs/GaAlAs dots and separately all In(Ga)As dots have a common value of δV_{HL} despite a spread in QD sizes, shape distortion, and alloy composition, suggesting that these factors do not influence significantly the coupling matrix δV_{HL}, in contrast with earlier expectations [5].

We could also deduce single-dot δV_{HL} by inserting precise numerical results of λ_{LH} and Δ_{HL} of a specific QD into

Eq. (1), for unstrained QDs, in terms of classical perturbation theory. Figure 4(b) shows such a computed single dot $\delta V_{\rm HL}$ of Gaussian-shaped GaAs QDs with varying dot height but the base size fixed to 25 nm, and all values lie around $\delta V_{\rm HL} = 2.15$ meV. This good agreement demonstrates the existence of a common coupling matrix $\delta V_{\rm HL}$ for all QDs within a class of QDs. We also validate the common coupling matrix $\delta V_{\rm HL} = 9.82$ meV for strained lens-shaped InAs QDs by inserting $\lambda_{\rm LH}$ and $\Delta_{\rm HL}$ of a specific QD into Eq. (2) to obtain single-dot $\delta V_{\rm HL}$, as shown in Fig. 4(b).

IV. DISCUSSION OF THE SUPERCOUPLING EFFECT

The reduction of effective HH-LH splitting in Eq. (2) implies a previously unrecognized effect that will be called "supercoupling," whereby a highly dense manifold of HH-like QD states lying energetically between the HH0 and LH0 states, evidenced clearly in our directly calculated eigenvalue spectrum for strained dots (Fig. 2), mediates the HH-LH coupling and significantly enhances the mixing by reducing the energy denominator $\Delta_{\rm HL}$ to a smaller value $\Delta_{\rm HL} - \delta$. We see in Fig. 2(b)—but not in Fig. 2(a), where the LH0 state is adjacent to the HH0 state—a dense manifold of states, derived predominantly from the bulk HH band, lying between HH0 and LH0 states. We postulate that these HH-like intermediate states form a ladder of the supercoupling between HH0 and LH0. This supercoupling effect is identical for all QDs within an entire class (or ensemble), reflecting a common $\delta = 78.6$ meV for all strained In(Ga)As QDs despite varying dot sizes, shape distortions, and alloy compositions, whenever the fluctuation in the number of intermediate states is small ($\sim$1%).

It should be noted that for strained In(Ga)As QDs, the curve is only fitted to 11 QDs, indicated by red dots (presented elsewhere [36]), and the remaining 25 QDs, indicated by red circles, are added after fitting and thus represent (predictions) of the simple formula. Because of the large HH-LH splitting in strained QDs, the supercoupling effect (reflected in the denominator $\Delta_{\rm HL}$) will dominate the HH-LH mixing over the direct coupling between HH0 and LH0 (reflecting in the numerator $\delta V_{\rm HL}$). Specifically, in the absence of supercoupling, i.e., $\delta = 0$, the magnitude of the HH-LH mixing, $\lambda^2_{\rm LH}$, will tend to less than 1% instead of the 5–20% predicted in strained In(Ga)As QDs, even though the built-in strain significantly enhances the coupling matrix $\delta V_{\rm HL}$ by a factor of 4.5 with respect to unstrained GaAs QDs.

The supercoupling is further confirmed by the presence of an abnormal point within the class of C_{2v} GaAs QDs (indicated by dot no. 1 in Fig. 3). This QD is embedded in AlAs instead of the $Al_{0.3}Ga_{0.7}As$ matrix, and it has a Gaussian shape with 25 nm base size and 3 nm height. A HH-like excited state HH1 is located *between* HH0 and LH0 in energy, and it has 4 meV energy separation from the LH0. For this specific QD, the coupling between HH0 and LH0 is mediated by the HH1, whereas in the remaining Gaussian-shaped QDs the state HH0 is immediately followed by LH0 without an intermediate state to mediate the interaction. Consequently, the HH-LH coupling is rather different in dots with and without intermediate states. In addition, there are dots with intermediate states but with small energy separation from the LH0, leading to a small supercoupling effect. For example, in the four lens-shaped GaAs/$Al_{0.3}Ga_{0.7}As$ QDs, the HH1 state is also located between HH0 and LH0, as shown in Fig. 2(c), but this level is closer to the LH0 with a smaller energy separation of less than 2 meV. Such a small energy separation leads to a very small supercoupling effect in these lens-shaped GaAs QDs, which is consistent with their points being insignificant away from the fitted line, as shown in Fig. 3.

The origin of the supercoupling effect. We now turn to examine the supercoupling effect mediated by intermediate states in the language of classic "folded down" descriptions [1–7,11–14,16,23]. In terms of perturbation theory, the Hamiltonian of a C_{2v} QD could be divided into two parts: $H_{C_{2v}} = H_0 + \delta V_{C_{2v}}$, where H_0 is the bare Hamiltonian with eigenstates of unperturbed HH and LH states: $\{E^0_{\rm HHn}, |\Psi^0_{\rm HHn}\rangle\}$ and $\{E^0_{\rm LHn}, |\Psi^0_{\rm LHn}\rangle\}$ $(n = 0,1,2,\dots)$. The perturbation potential $\delta V_{C_{2v}}$ lowers the QD symmetry to C_{2v} and hence introduces HH-LH mixing, which modifies the ground hole state HH0 [1–7,11–14,16,18,23],

$$|\Psi'_{\rm HH0}\rangle = \left|\Psi^0_{\rm HH0}\right\rangle + \sum_m \frac{\left\langle\Psi^0_{\rm LHm}\left|\delta V_{C_{2v}}\right|\Psi^0_{\rm HH0}\right\rangle}{E^0_{\rm HH0} - E^0_{\rm LHm}}\left|\Psi^0_{\rm LHm}\right\rangle. \quad (3)$$

In the above equation, one usually takes LH0 into account and neglects the LH excited states [1–7,11–14,16,18,23] considering they are far from HH0 compared with LH0. Consequently,

$$\lambda_{\rm LH} = \frac{\left\langle\Psi^0_{\rm LH0}\left|\delta V_{C_{2v}}\right|\Psi^0_{\rm HH0}\right\rangle}{E^0_{\rm HH0} - E^0_{\rm LH0}} = \frac{\delta V_{\rm HL}}{\Delta_{\rm HL}}. \quad (4)$$

In strained nanostructures, say In(Ga)As/GaAs QDs, there is a dense manifold of HH-like intermediate states lying in energy between HH0 and LH0, as observed in sophisticated calculations including multiband $\mathbf{k}\cdot\mathbf{p}$ approaches [19] and atomistic calculations [27–30] and shown in Fig. 2(b). These intermediate HH-like states, neglected in classical model Hamiltonian treatments [1–7,11–14,16,23], are also allowed to couple to HH0 under C_{2v} symmetry, and further modify the ground hole state,

$$|\Psi''_{\rm HH0}\rangle = |\Psi'_{\rm HH0}\rangle + \sum_{n\geq 1} \frac{\langle\Psi'_{\rm HHn}|\delta V_{C_{2v}}|\Psi'_{\rm HH0}\rangle}{E'_{\rm HH0} - E'_{\rm HHn}}|\Psi'_{\rm HHn}\rangle, \quad (5)$$

where $|\Psi'_{\rm HH0}\rangle$ is given in Eq. (3) and $|\Psi'_{\rm HHn}\rangle$ $(n = 1,2,\dots)$ is straightforward to get by replacing HH0 with HHn in Eq. (3). Inserting the equations for $|\Psi'_{\rm HHn}\rangle$ into Eq. (5), we are ready to obtain the revised $\lambda_{\rm LH0}$,

$$\lambda_{\rm LH0} = \frac{\left\langle\Psi^0_{\rm LH0}\left|\delta V_{C_{2v}}\right|\Psi^0_{\rm HH0}\right\rangle}{E^0_{\rm HH0} - E^0_{\rm LH0}} + \sum_{n\geq 1}\frac{\left\langle\Psi^0_{\rm LH0}\left|\delta V_{C_{2v}}\right|\Psi^0_{\rm HHn}\right\rangle}{E^0_{\rm HHn} - E^0_{\rm LH0}} \cdot \frac{\left\langle\Psi^0_{\rm HHn}\left|\delta V_{C_{2v}}\right|\Psi^0_{\rm HH0}\right\rangle}{E'_{\rm HH0} - E'_{\rm HHn}} + O(E^{-3}). \quad (6)$$

The additional terms mediated by HH-like excited states HHn can be approximately regarded as higher-order terms of a Taylor series of

$$\lambda_{\rm LH0} = \frac{\left\langle\Psi^0_{\rm LH0}\left|\delta V_{C_{2v}}\right|\Psi^0_{\rm HH0}\right\rangle}{E^0_{\rm HH0} - E^0_{\rm LH0} - \delta} = \frac{\delta V_{\rm HL}}{\Delta_{\rm HL} - \delta}. \quad (7)$$

The parameter δ is adjustable to accommodate the difference of Eq. (6) from a Taylor series. It is now clear that reduction in the

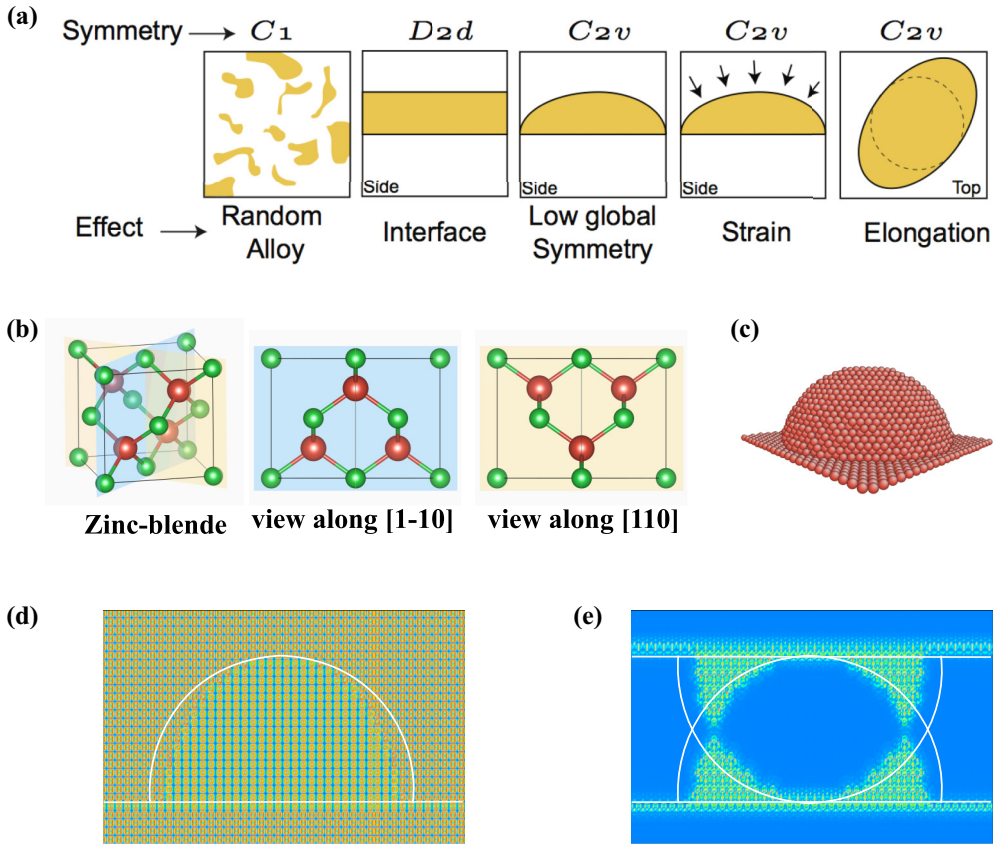

FIG. 5. (Color online) Illustrations of the effects leading to nonvanishing HH-LH coupling. (a) Schematic illustration of five out of the six possible physical effects leading to a nonvanishing direct HH-LH coupling matrix element $\delta V_{\rm HL}$. (b) ZB crystal structure with views along the $[1\bar{1}0]$ and [110] directions. The yellow and blue planes represent the crystal (110) and $(1\bar{1}0)$ planes. (c) Schematic of a lens-shaped GaAs QD sitting on a 1-ML-thick GaAs wetting layer. (d) Absolute difference of the crystal potential, of the QD defined in (c), in the (110) plane and in the $(1\bar{1}0)$ plane. Red for maximum and blue for zero value. The expected potential difference is zero if the QD has D_{2d} symmetry, as supposed in continuum theory. (e) Absolute difference of the crystal potential in the (110) plane and the potential in the $(1\bar{1}0)$ plane but after a reflection operation about the (001) mirror plane. The areas of finite values near the interfaces of the QD show, therefore, deviations from D_{2d} symmetry.

denominator $\Delta_{\rm HL}$ by δ originates from the indirect coupling between HH0 and LH0 mediated by HH-like excited states, in analogy with the well-known superexchange magnetic interaction through a nonmagnetic anion [37]. We refer to this indirect coupling channel as "supercoupling."

V. DIRECT HH-LH COUPLING EFFECTS

Having discussed the denominator effect $\Delta_{\rm HL}$ quantifying the enhancement of HH-LH mixing through the supercoupling mechanism via HH-like intermediate QD states, we turn to discuss the numerator effect $\delta V_{\rm HL}$ quantifying the relative importance of distinct factors in direct HH-LH coupling. An important observation here is the role of atomically resolved symmetry versus global shape symmetry. As shown in Figs. 5(b)–5(e), the symmetry of ideally shaped (circular based lens-, cone-, and Gaussian-shape) self-assembled QDs made of common ZB structure semiconductors is already lowered to C_{2v} as evidenced by the nonequivalence of the crystal along the [110] and $[1\bar{1}0]$ directions, illustrated in Fig. 5(d). QDs are distinct from bulk ZB crystals or D_{2d} symmetric (001) quantum wells, where the [110] direction can be transformed into the $[1\bar{1}0]$ direction by S_4 symmetry operations (90° rotation followed by a reflection [38]). Thus, whereas in the bulk ZB or D_{2d} systems symmetry forbids HH-LH mixing, in ideally shaped self-assembled QDs embedded in a matrix, *the HH-LH mixing is intrinsically allowed* even without built-in strain or QD shape nonideality (anisotropy). The six mechanisms that contribute to the direct HH-LH coupling $\delta V_{\rm HL}$ are analyzed and quantified next.

(i) 3D confinement of wave functions in QDs has only a negligible effect on δV_{HL}. In terms of the Luttinger-Kohn Hamiltonian or the Pikus-Bir strain Hamiltonian, which is briefly introduced in the Appendix, the HH-LH mixing in 3D bulk is absent at the Γ point but present away from the Γ point, due to the off-diagonal band coupling terms R and S that are proportional to $\mathbf{k}$ and are finite away from the Γ point. Whereas in 0D QDs $\mathbf{k}_i$ is replaced by the operator $-i\frac{\partial}{\partial r_i}$ $(i = x,y,z)$ as a result of space confinement, the ground state has an effective finite wave vector that leads to finite R and S and thus $\delta V_{\rm HL} \neq 0$. Such 3D quantum confinement was previously considered as the only mechanism leading to HH-LH mixing in unstrained QDs [5,14,21–23]. For flat GaAs QDs [where a_z(height) $\ll L$(wide)], 3D confinement within the Luttinger-Kohn Hamiltonian gives rise to $\lambda_{\rm LH} \simeq 0.53 a_z/L$ [5] and $\lambda^2_{\rm LH} = 0.2\%$, a much smaller value than our determined 3.5%,

for a disk-shaped dot with $a_z = 2$ nm, $L = 25$ nm, as shown in Fig. 4(a). Furthermore, Fig. 4(b) shows that in atomistic calculations, $\lambda^2_{\rm LH}$ is nearly insensitive to the QD height for both disk-shaped and lens-shaped GaAs/Al(Ga)As QDs, in contrast with the model Hamiltonian result of $\lambda^2_{\rm LH} \simeq (a_z/L)^2$. These discrepancies illustrate the negligible effect of 3D confinement on $\delta V_{\rm HL}$ and in turn on HH-LH mixing in flat QDs, since all possible factors are included in our atomistic calculations, but only 3D confinement is included in the model Hamiltonian. Note that the atomistic symmetry of QDs, which was usually overlooked in the simple $\mathbf{k}\cdot\mathbf{p}$ calculations, ultimately controls the possibility of the HH-LH mixing: even when R and S terms are finite, the HH-LH mixing should be absent if symmetry forbids such mixing; the well-known HH-LH mixing away from Γ point in 3D bulk is not only due to finite R and S, but also to the reduced symmetry at these k points.

(ii) Shape anisotropy (e.g., in-plane elongation) in QDs has only a small effect on δV_{HL}. The in-plane shape anisotropy [Fig. 5(a)] can lower the QD symmetry from D_{2d} to C_{2v} leading to nonzero $\delta V_{\rm HL}$ and hence enhancing the HH-LH mixing. In the approximation of the Luttinger-Kohn Hamiltonian, the contribution of QD shape anisotropy to $\delta V_{\rm HL}$ is described by the R term associated with $k_x^2 - k_y^2$, and it is L/a_z times smaller than the contribution from space confinement of the S term associated with k_z [39]. In self-assembled QDs, where the dot height a_z is usually much smaller than the base size L, the shape anisotropy effect on $\delta V_{\rm HL}$ is negligible in comparison to the quantum confinement effect. This negligible effect assures the validation of the predicted common $\delta V_{\rm HL}$ by atomistic calculations for a class of QDs despite dot-shape anisotropy. Figure 3 shows a common $\delta V_{\rm HL} = 2.15$ meV for the class of self-assembled unstrained C_{2v} GaAs QDs and a common $\delta V_{\rm HL} = 9.82$ meV for the class of strained InAs QDs. In the class of 31 C_{2v} GaAs QDs, there are 10 shape anisotropic dots (half elongated along the $[1\bar{1}0]$ direction and half along the [110] direction). In the class of 36 C_{2v} In(Ga)As QDs, there are 12 dots possessing shape elongation. This finding highlights the incorrect link often drawn between HH-LH mixing and shape anisotropy, whereby one infers shape anisotropy from measuring the HH-LH mixing [8,13,40,41].

(iii) Built-in strain does not lower the symmetry but significantly enhances δV_{HL}. In the classical Pikus-Bir strain Hamiltonian [39,42], the shear strain components (ϵ_{xy}, ϵ_{yz}, and ϵ_{zx}), belonging to rhombohedral symmetries, give rise to finite off-diagonal R and S terms (see the Appendix for details), which will mix HH and LH if such mixing is allowed by symmetry. These shear components are absent in 3D bulk with D_{2d} or C_{2v} symmetry, but they are present at the interfaces of QDs. From an atomistic point of view the built-in strain does not lower the symmetry, and as such it is not the reason for allowing the HH-LH mixing. However, such built-in strain through atomic relaxation allows the local asymmetry of the interface to propagate inside the QD, where the wave functions are localized [27]. The increase in $\delta V_{\rm HL}$ (from 2.15 to 9.82 meV), from unstrained GaAs/Al(Ga)As QDs to strained In(Ga)As/GaAs QDs as shown in Fig. 2(a), is mainly due to the built-in strain. We conclude that the built-in strain constitutes an important contribution to the coupling [$(9.82 - 2.15)/9.82 = 78\%$ in strained QDs] if HH-LH mixing is allowed by symmetry.

(iv) Alloy disorder in the QD material or its matrix has only a small effect on δV_{HL}: Although the alloy randomness is important for both exciton fine-structure splitting [4] and optical polarization [28] in QDs, it has a negligible effect on HH-LH mixing, as demonstrated here by the fact that both ordered InAs/GaAs and disordered $In_{60}Ga_{40}As$/GaAs QDs share the same $\delta V_{\rm HL} = 9.82$ meV, and both ordered GaAs/AlAs and disordered GaAs/$Al_{30}Ga_{70}As$ QDs share the same $\delta V_{\rm HL} = 2.15$ meV. Moreover, five different random alloy realizations of a Gaussian-shaped 3-nm-high GaAs/$Al_{30}Ga_{70}As$ QD lead to virtually the same coupling, $\lambda^2_{\rm LH} = 13.3\%$, 13.0%, 12.9%, 13.1%, and 12.8%, with a standard deviation of $\sigma = 0.2\%$. Also, five different random alloy realizations of $In_{60}Ga_{40}As$/GaAs QDs give rise to four $\lambda^2_{\rm LH} = 3.6\%$ and one $\lambda^2_{\rm LH} = 3.8\%$. This strongly suggests the negligible effect of alloy disorder on HH-LH mixing and $\delta V_{\rm HL}$.

(v) A significant effect of low-symmetry interfaces on δV_{HL}: (001) quantum wells BAB with global D_{2d} symmetry consist of two interfaces B-A and A-B each having a lower C_{2v} local symmetry. When both C_{2v} interfaces are considered simultaneously, the mirror plane operation in the well center joins them into the higher D_{2d} point group. A periodic bulk material with this symmetry has zero HH-LH mixing at the Γ point. It was recognized long ago [18] that the local C_{2v} symmetry of each interface in a quantum well gives rise to HH-LH mixing. We have considered the analogous situation in nominal D_{2d} (disk-shaped) GaAs QDs embedded in $Al_{30}Ga_{70}As$ barriers by performing atomistic pseudopotential calculations. Because of the negligible effects of space confinement and alloy disorder, the obtained $\delta V_{\rm HL} = 0.8$ meV for D_{2d} (disk-shaped) GaAs QDs, as shown in Fig. 4, is due predominantly to the local C_{2v} interface effect. This effect represents around $0.8/2.15 \sim 40\%$ of the total coupling strength $\delta V_{\rm HL}$ in unstrained C_{2v} GaAs QDs and $0.8/9.82 \sim 8\%$ in strained InAs QDs.

(vi) Effect of the intrinsic C_{2v} symmetry of symmetric QDs on δV_{HL} due to the inequivalence of the [110] and $[1\bar{1}0]$ directions. The atomistic symmetry of ideal circular-based lens-shape or Gaussian-shape QDs is C_{2v}, and therefore it is lower than in the previously discussed quantum-well case, because the [110] and $[1\bar{1}0]$ directions are nonequivalent due to the upper curved interface, which is illustrated in Figs. 5(d) and 5(c). The curvature introduced in the top interface corresponds to a lowering of the global symmetry, from a disk-shaped QD with global D_{2d} symmetry to a lens-shaped QD with a global C_{2v} symmetry. We attribute the increase in $\delta V_{\rm HL}$ from disk-shaped QDs [$\delta V_{\rm HL} = 0.8$ meV, green squares in Fig. 4(b)] to lens-shaped QDs [$\delta V_{\rm HL} = 2.15$ meV, blue triangles in Fig. 4(b)] to the intrinsic C_{2v} symmetry due to the bending of the top interface, i.e., due to an asymmetry in the growth direction. We therefore conclude that the intrinsic C_{2v} symmetry of symmetric QDs is responsible for 60% of $\delta V_{\rm HL}$ in unstrained C_{2v} GaAs/AlGaAs QDs and 14% $\delta V_{\rm HL}$ in strained InGaAs/GaAs QDs.

VI. CONCLUSION

We discovered a mechanism of HH-LH mixing, termed supercoupling, that emerged naturally from atomistic pseudopotential calculations on a range of strained and unstrained QDs of different symmetries. The supercoupling between HH

and LH in self-assembled QDs is analogous to superexchange in magnetism in that it is remarkably enhanced by the presence in the QD of a dense ladder of intermediate states, which amplifies and propagates the coupling across a significant energy window separating the primary HH0 and LH0 states. Because the supercoupling effect is only associated with intermediate states between HH0 and LH0 states whenever HH-LH mixing is allowed, conclusions drawn here based on self-assembled QDs are also applicable for other nanostructures, including quantum wires, quantum wells, and heterojunctions.

In addition to the supercoupling, which contributes to the HH-LH mixing through the denominator effect Δ_{HL}, there are six "direct coupling" effects in QDs contributing to the HH-LH mixing through the numerator δV_{HL}, including (i) space confinement, (ii) dot shape anisotropy, (iii) built-in strain, (iv) alloy disorder, (v) local symmetry of interfaces, and (vi) intrinsic C_{2v} crystal field. We quantify that in *unstrained* self-assembled QDs, effects (i)–(vi) contribute 0%, 0%, 0%, 0%, 40%, and 60%, respectively, whereas in *strained* self-assembled QDs they contribute 0%, 0%, 78%, 0%, 8%, and 14% to the direct HH-LH coupling δV_{HL}. However, the supercoupling effect, via dense intermediate QD states, is the dominant mechanism for finite HH-LH mixing in strained QDs. Only the reduction of the denominator as a consequence of supercoupling can lead to the HH-LH mixing λ^2_{LH} values we obtain from our atomistic calculations.

ACKNOWLEDGMENTS

J.W.L. was supported by the National Young 1000 Talents Plan and the National Natural Science Foundation of China (NSFC Grant No. 61474116). A.Z. was supported by the Office of Science, Basic Energy Science, MSE division under Grant No. DE-FG02-13ER46959 to CU Boulder. G.B. was supported by the BMBF (QuaHL-Rep, Contract No. 01BQ1034).

APPENDIX: LUTTINGER-KOHN AND PIKUS-BIR HAMILTONIANS

Although we believe that a sufficiently complete basis set $\mathbf{k}\cdot\mathbf{p}$ approach might be able to correctly treat HH-LH mixing, the comparisons between direct atomistic pseudopotential calculations and Luttinger-Kohn and Pikus-Bir Hamiltonians enable us to unravel the contributions of factors missing in simple $\mathbf{k}\cdot\mathbf{p}$ to HH-LH mixing. Furthermore, the most popular approach for studying nanostructures is by folding the Luttinger-Kohn or Pikus-Bir strained multiband hole Hamiltonian of bulk ZB semiconductors down to an effective 2×2 HH Hamiltonian and taking the admixture of neighboring bands such as the LH band into account perturbatively [5]. According to Pikus and Bir [39], the correspondence between the strain Hamiltonian and the Luttinger-Kohn Hamiltonian is

$$k_i k_j \leftrightarrow e_{ij}, \tag{A1}$$

therefore the total Hamiltonian $H = H_{\mathbf{k}\cdot\mathbf{p}} + H_{\mathrm{strain}}$ describing the top of the valence band for bulk ZB or diamond semiconductors under strain e is given by

$$H = \begin{pmatrix} P+Q & -S & R & 0 \\ -S^\dagger & P-Q & 0 & R \\ R^\dagger & 0 & P-Q & S \\ 0 & R^\dagger & S^\dagger & P+Q \end{pmatrix}, \tag{A2}$$

where the spin-orbit split-off band is ignored, and all matrix elements are written in terms of three dimensionless Luttinger parameters γ_1, γ_2, and γ_3 and three deformation potentials a, b, and d:

$$P = \frac{\hbar^2}{2m}\gamma_1 k^2 - a_v(e_{xx}+e_{yy}+e_{zz}), \tag{A3}$$

$$Q = \frac{\hbar^2}{2m}\gamma_2\left(k_x^2+k_y^2-2k_z^2\right) - \frac{b}{2}(e_{xx}+e_{yy}-2e_{zz}), \tag{A4}$$

$$S = \frac{\hbar^2}{2m}2\sqrt{3}\gamma_3(k_x - ik_y)k_z - d(e_{xz}-ie_{yz}), \tag{A5}$$

$$R = \frac{\hbar^2}{2m}\sqrt{3}\left[-\gamma_2\left(k_x^2-k_y^2\right)+2i\gamma_3 k_x k_y\right] + \frac{\sqrt{3}}{2}b(e_{xx}-e_{yy}) - ide_{xy}. \tag{A6}$$

The basis vectors are the four degenerate Bloch wave functions (HH and LH bands) at the center of the Brillouin zone:

$$|3/2,3/2\rangle = -\frac{1}{\sqrt{2}}|(X+iY)\uparrow\rangle, \tag{A7}$$

$$|3/2,1/2\rangle = \frac{1}{\sqrt{6}}|-(X+iY)\downarrow+2Z\uparrow\rangle, \tag{A8}$$

$$|3/2,-1/2\rangle = \frac{1}{\sqrt{6}}|(X-iY)\uparrow+2Z\downarrow\rangle, \tag{A9}$$

and

$$|3/2,-3/2\rangle = \frac{1}{\sqrt{2}}|(X-iY)\downarrow\rangle. \tag{A10}$$

[1] Y. H. Huo *et al.*, Nat. Phys. **10**, 46 (2014).
[2] A. J. Bennett, M. A. Pooley, R. M. Stevenson, M. B. Ward, R. B. Patel, A. B. de la Giroday, N. Skold, I. Farrer, C. A. Nicoll, D. A. Ritchie *et al.*, Nat. Phys. **6**, 947 (2010).
[3] M. Ghali, K. Ohtani, Y. Ohno, and H. Ohno, Nat. Commun. **3**, 661 (2012).
[4] J.-W. Luo, R. Singh, A. Zunger, and G. Bester, Phys. Rev. B **86**, 161302 (2012).
[5] J. Fischer and D. Loss, Phys. Rev. Lett. **105**, 266603 (2010).
[6] E. A. Chekhovich, M. N. Makhonin, A. I. Tartakovskii, A. Yacoby, H. Bluhm, K. C. Nowack, and L. M. K. Vandersypen, Nat. Mater. **12**, 494 (2013).
[7] R. J. Warburton, Nat. Mater. **12**, 483 (2013).
[8] C. Testelin, F. Bernardot, B. Eble, and M. Chamarro, Phys. Rev. B **79**, 195440 (2009).
[9] B. Eble, C. Testelin, P. Desfonds, F. Bernardot, A. Balocchi, T. Amand, A. Miard, A. Lemaitre, X. Marie, and M. Chamarro, Phys. Rev. Lett. **102**, 146601 (2009).

[10] J.-W. Luo, A. N. Chantis, M. van Schilfgaarde, G. Bester, and A. Zunger, Phys. Rev. Lett. **104**, 066405 (2010).
[11] A. V. Koudinov, I. A. Akimov, Y. G. Kusrayev, and F. Henneberger, Phys. Rev. B **70**, 241305 (2004).
[12] K. Kowalik, O. Krebs, A. Lemaître, J. A. Gaj, and P. Voisin, Phys. Rev. B **77**, 161305 (2008).
[13] T. Belhadj, T. Amand, A. Kunold, C.-M. Simon, T. Kuroda, M. Abbarchi, T. Mano, K. Sakoda, S. Kunz, X. Marie *et al.*, Appl. Phys. Lett. **97**, 051111 (2010).
[14] Y.-H. Liao, C.-C. Liao, C.-H. Ku, Y.-C. Chang, S.-J. Cheng, M. Jo, T. Kuroda, T. Mano, M. Abbarchi, and K. Sakoda, Phys. Rev. B **86**, 115323 (2012).
[15] C. Tonin, R. Hostein, V. Voliotis, R. Grousson, A. Lemaitre, and A. Martinez, Phys. Rev. B **85**, 155303 (2012).
[16] F. Fras, F. Bernardot, B. Eble, M. Bernard, B. Siarry, A. Miard, A. Lemaitre, C. Testelin, and M. Chamarro, J. Phys.: Condens. Matter **25**, 202202 (2013).
[17] X. Xu, Y. Wu, B. Sun, Q. Huang, J. Cheng, D. G. Steel, A. S. Bracker, D. Gammon, C. Emary, and L. J. Sham, Phys. Rev. Lett. **99**, 097401 (2007).
[18] E. L. Ivchenko, A. Y. Kaminski, and U. Rössler, Phys. Rev. B **54**, 5852 (1996).
[19] O. Stier, M. Grundmann, and D. Bimberg, Phys. Rev. B **59**, 5688 (1999).
[20] R. Winkler, *Spin-Orbit Coupling Effects in Two-Dimensional Electron and Hole Systems*, Vol. 191 of Springer Tracts in Modern Physics (Springer-Verlag, Berlin, 2003).
[21] S.-S. Li, J.-B. Xia, Z. L. Yuan, Z. Y. Xu, W. Ge, X. R. Wang, Y. Wang, J. Wang, and L. L. Chang, Phys. Rev. B **54**, 11575 (1996).
[22] T. Tanaka, J. Singh, Y. Arakawa, and P. Bhattacharya, Appl. Phys. Lett. **62**, 756 (1993).
[23] Y. Y. Léger, L. Besombes, L. Maingault, and H. Mariette, Phys. Rev. B **76**, 045331 (2007).
[24] F. Vouilloz, D. Y. Oberli, M.-A. Dupertuis, A. Gustafsson, F. Reinhardt, and E. Kapon, Phys. Rev. B **57**, 12378 (1998).
[25] F. Vouilloz, D. Y. Oberli, M.-A. Dupertuis, A. Gustafsson, F. Reinhardt, and E. Kapon, Phys. Rev. Lett. **78**, 1580 (1997).
[26] C. Pryor, J. Kim, L. W. Wang, A. J. Williamson, and A. Zunger, J. Appl. Phys. **83**, 2548 (1998).
[27] G. Bester and A. Zunger, Phys. Rev. B **71**, 045318 (2005).
[28] V. Mlinar, M. Bozkurt, J. M. Ulloa, M. Ediger, G. Bester, A. Badolato, P. M. Koenraad, R. J. Warburton, and A. Zunger, Phys. Rev. B **80**, 165425 (2009).
[29] L.-W. Wang and A. Zunger, Phys. Rev. B **59**, 15806 (1999).
[30] A. J. Williamson, L.-W. Wang, and A. Zunger, Phys. Rev. B **62**, 12963 (2000).
[31] H. Fu, L. W. Wang, and A. Zunger, Phys. Rev. B **57**, 9971 (1998).
[32] L. W. Wang and A. Zunger, Phys. Rev. B **54**, 11417 (1996).
[33] L. W. Wang, A. J. Williamson, A. Zunger, H. Jiang, and J. Singh, Appl. Phys. Lett. **76**, 339 (2000).
[34] J.-W. Luo, G. Bester, and A. Zunger, Phys. Rev. B **79**, 125329 (2009).
[35] G. Bester, S. Nair, and A. Zunger, Phys. Rev. B **67**, 161306 (2003).
[36] J. W. Luo, G. Bester, and A. Zunger, in *Atomistic Pseudopotential Theory of Droplet Epitaxial GaAs/AlGaAs Quantum Dots*, in *Nanodroplets*, edited by Z. M. Wang, Lecture Notes in Nanoscale Science and Technology Vol. 18 (Springer, New York, 2013), pp. 329–361.
[37] P. W. Anderson, Phys. Rev. **79**, 350 (1950).
[38] G. Koster, J. Dimmock, R. Wheeler, and H. Statz, *Properties of the Thirty-two Point Groups* (MIT Press, Cambridge, MA, 1963).
[39] G. Bir and G. Pikus, *Symmetry and Strain-Induced Effects in Semiconductors* (Wiley, New York, 1974).
[40] S. Moehl, I. C. Robin, Y. Léger, R. André, L. Besombes, and K. Kheng, Phys. Status Solidi B **243**, 849 (2006).
[41] J. Fernández-Rossier, Phys. Rev. B **73**, 045301 (2006).
[42] S.-H. Wei and A. Zunger, Phys. Rev. B **49**, 14337 (1994).